

# Computation lithography: virtual reality and virtual virtuality

Alfred K. K. Wong<sup>a</sup> and Edmund Y. Lam<sup>b</sup>

<sup>a</sup>Magma Design Automation, Inc., 1650 Technology Drive, San Jose, CA 95110, U. S. A.

<sup>b</sup>Department of EEE, The University of Hong Kong, Pokfulam Road, Hong Kong\*

## Abstract

Computation lithography is enabled by a combination of physical understanding, mathematical abstraction, and implementation simplification. An application in the virtual world of computation lithography can be a virtual reality or a virtual virtuality depending on its engineering sensible-ness and technical feasibility.

## 1 Introduction

The current prevalence of computation lithography traces its root to the 1970s, when it was discovered that photoresist dissolution can be modeled as a surface etching phenomena, with the etch rate dependent on the state of photochemistry rather than the manner in which the resist was exposed.<sup>1,2</sup> But it has taken some time before lithography simulation, the precursor of computation lithography, establishes its present-day credibility.<sup>1</sup> Even as late as the 1980s lithography simulation was still labeled by some as “Yesterday’s technology simulated tomorrow”.<sup>5</sup>

Nevertheless, the 1970s and 1980s was a germinating period for lithography simulation; many fundamental algorithms were developed. Computation of partially coherent imaging was placed on a firm foundation,<sup>6</sup> permitting accurate simulation of projection printing in the regime where neither the relationship between mask and intensity nor that between objects and image-plane field is linear. A variety of techniques, including the waveguide method,<sup>7,8</sup> and finite-element<sup>9,10</sup> and finite-difference approaches,<sup>11,12</sup> were developed to examine scattering and diffraction of light propagation through mask openings. Resist development modeling, which had been plagued by looping instability in which surfaces of dissolved materials curve back onto itself,<sup>13</sup> was properly handled by the fast-marching level-set method.<sup>13,14</sup>

These algorithms enhanced a lithographer’s arsenal of tools, complementing empirical data supplied by wafer exposures. With exponential improvement in computer speed and rising equipment cost, simulation imperceptibly assumed an ever-increasing role in lithography process development. During the 1970s and 1980s, however, algorithm performance still restricted analysis to dimensions on the order of a feature size.

Adoption of optical proximity correction (OPC) in the 1990s triggered further innovation. Success of rule-based OPC<sup>15,16</sup> quickly translated to a demand for model-based OPC,<sup>17-20</sup> which clamored full-chip image computation capabilities. Coherent decomposition<sup>21-23</sup> was equal to the challenge. By approximating a partially coherent optical system as a weighted collection of coherent systems, computation complexity was reduced by orders of magnitude.

## 2 Ingredients of computation lithography

Model-based OPC is an epitome of computation lithography, which can be defined as the use of computer algorithms in lithography-related integrated circuit (IC) development. The basic components of a computation lithography application are

---

\*The work described in this paper was partially supported by two grants from the Research Grants Council of the Hong Kong Special Administrative Region, China (Project Numbers 713906 and 713408).

<sup>1</sup>The history of lithography simulation is considered from a few points of view in Dill,<sup>3</sup> Mack,<sup>4</sup> and Neureuther.<sup>5</sup>

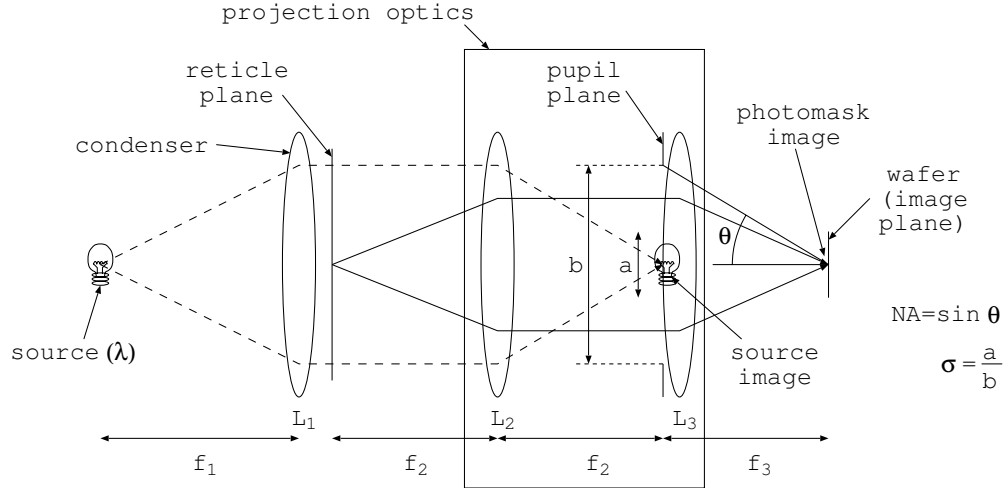


Figure 1: Illustration of a projection microlithography exposure system.<sup>26</sup>

1. specifications;
2. physical understanding;
3. mathematical abstraction; and
4. implementation simplification.

Let us illustrate these aspects using full-chip image computation as an example.

## 2.1 Specifications

The goal of full-chip image computation is to calculate the image intensities at select locations (or critical dimensions of select features) on a design quickly and accurately. Depending on the application, “quickly” and “accurately” are specified by concrete numbers such as 1 s per intensity value and 1 nm maximum deviation from empirical calibration data.

## 2.2 Physical understanding

In order to compute an image, a comprehension of image formulation principles is necessary. From an understanding of light diffraction, the physics of a projection microlithography system can be distilled, as illustrated in Fig. 1.<sup>24,25</sup> A quasi-monochromatic light source of mean wavelength  $\lambda$  illuminates the reticle via the condenser lens  $L_1$ . In conjunction with  $L_1$ , the lens  $L_2$  forms an image of the source in the pupil. This lens  $L_2$  performs a Fourier transform of the object such that the field across the pupil plane is the spectrum of the object. Low-spatial-frequency components pass closer to the center of the pupil, and higher-frequency components are nearer to the periphery of the pupil. The highest frequencies are cut off by the pupil. The lens  $L_3$  forms the image by combining the filtered frequency components.

## 2.3 Mathematical abstraction

Before an algorithm for image computation can be formulated, operation of the exposure system depicted in Fig. 1 needs to be described mathematically. Image intensity at a point  $(x, y)$  is given by:<sup>27</sup>

$$I(x, y) = \iiint_{-\infty}^{+\infty} \iiint_{-\infty}^{+\infty} w(x - x'_o, y - y'_o; x - x''_o, y - y''_o) O(x'_o, y'_o) O^*(x''_o, y''_o) dx'_o dy'_o dx''_o dy''_o, \quad (1)$$

where

$$\begin{aligned}
 w(x'_o, y'_o; x''_o, y''_o) &= J(x'_o - x''_o, y'_o - y''_o)H(x'_o, y'_o)H^*(x''_o, y''_o), \\
 J(x'_o - x''_o, y'_o - y''_o) &\text{ is the mutual intensity,} \\
 H(x, y) &\text{ is the optical system transfer function,} \\
 O(x, y) &\text{ is the mask transmittance,}
 \end{aligned}$$

and the asterisk \* represents complex conjugation. Equation (1) says that the image intensity at  $(x, y)$  can be interpreted as the weighted sum ( $w$ ) of contributions from neighboring objects  $O(x'_o, y'_o)$  and  $O(x''_o, y''_o)$ .

## 2.4 Implementation simplification

Computation complexity of Eq. (1) is high because of the four-fold integral. To improve efficiency, the function  $w$  can be decomposed into a series of its eigenvectors  $\varphi_k$  and corresponding eigenvalues  $\lambda_k$ ,<sup>21</sup> such that

$$w(x'_o, y'_o; x''_o, y''_o) = \sum_{k=1}^{\infty} \lambda_k \varphi_k(x'_o, y'_o) \varphi_k^*(x''_o, y''_o).$$

For typical exposure systems, the magnitudes of a few eigenvalues are much larger than the rest. We can thus approximate the image as a finite sum of, say,  $K$  dominant eigenvectors:

$$I(x, y) \cong \sum_{k=1}^K \lambda_k \left| \iint_{-\infty}^{+\infty} \varphi_k(x - x', y - y') O(x', y') dx' dy' \right|^2. \quad (2)$$

Although Eq. (2) reduces the four-fold integral of Eq. (1) to  $K$  two-dimensional convolutions, computation complexity is still high. Nevertheless, for layouts that can be decomposed exclusively into rectangles, we can represent each rectangle as the sum of four quadrant functions

$$Q(x, y) = \begin{cases} 1 & \text{if } x \geq 0 \text{ and } y \geq 0, \\ 0 & \text{otherwise,} \end{cases}$$

such that

$$\begin{aligned}
 O(x, y) = \sum_{n=1}^N t_{\text{fg}}^{(n)} [ & Q(x - x_1^{(n)}, y - y_1^{(n)}) - Q(x - x_2^{(n)}, y - y_1^{(n)}) + \\
 & Q(x - x_2^{(n)}, y - y_2^{(n)}) - Q(x - x_1^{(n)}, y - y_2^{(n)}) ],
 \end{aligned}$$

where  $N$  is the total number of rectangles, the superscript  $(n)$  indexes the rectangular shapes, and  $t_{\text{fg}}^{(n)}$  represents the transmittance of the  $n^{\text{th}}$  shape.<sup>22,23</sup> Substituting the above expression into Eq. (2) results in

$$\begin{aligned}
 I(x, y) \cong \sum_{k=1}^K \left| \sum_{n=1}^N [ & \psi_k(x - x_1^{(n)}, y - y_1^{(n)}) - \psi_k(x - x_2^{(n)}, y - y_1^{(n)}) + \\
 & \psi_k(x - x_2^{(n)}, y - y_2^{(n)}) - \psi_k(x - x_1^{(n)}, y - y_2^{(n)}) ] \right|^2, \quad (3)
 \end{aligned}$$

where

$$\psi_k(x, y) = \sqrt{\lambda_k} \cdot Q(x, y) \otimes \varphi_k(x, y)$$

is the convolution of the quadrant function with the  $k^{\text{th}}$  eigenvector scaled by the eigenvalue. Since the functions  $\psi_k(x, y)$  are independent of the object, they can be precomputed and stored. Image calculation hence becomes an addition operation, improving computation efficiency tremendously.

### 3 Virtual reality and virtual virtuality

In the virtual world of computation lithography, virtual realities are those applications that perform useful service for IC development. They are tools characterized by

1. specifications that make engineering sense, and
2. performance (based on physical understanding, mathematical abstraction, and implementation simplification) that meets the specification targets.

Virtual virtualities, on the other hand, are algorithms that fall short of one or both of the two criteria. That model-based OPC and post-OPC verification<sup>28,29</sup> are virtual realities there is little doubt; they are incumbents in a standard production flow. But it is of interest to examine the degree of reality of a few applications at the fringe.

#### 3.1 Inverse lithography

Inverse lithography aims to derive the optimal mask given a desired image.<sup>30,31</sup> Since the synthesized mask is unconstrained by the topology of the original physical design, inverse lithography promises to deliver superior performance over existing model-based OPC approaches. The specifications of inverse lithography make engineering sense, for they are essentially those of OPC's. However, current performance still falls short, primarily because of the lack of a mathematical description for mask regularization<sup>32</sup> that provides a satisfactory balance between lithography robustness and mask manufacturability.

In a similar manner, determining printability of a layout using a generic model<sup>33</sup> is hindered by deficiency of the mask model, and concurrent source-mask optimization<sup>34</sup> needs to resolve both mask and source regularization issues.

#### 3.2 Physical DFM

Physical design-for-manufacturability (DFM) refers to remedying weaknesses in a physical design.<sup>35</sup> It comprises finding hotspots by model-based verification, and fixing them by polygon movements. Since these two steps are rather straightforward, there is little implementation difficulty. The issue lies with specifications.

During the hotspot analysis stage in physical DFM, it is sometimes impractical, for turn-around or for accessibility reasons, to apply the same algorithm as the one used for sign-off verification. Differences between the DFM and the sign-off algorithms would result in hotspot discrepancy, leading to imperfect accuracy such as misses (hotspots not being remedied) and extraneous fixing (repairing of non-hotspots). The achievable accuracy depends on algorithm precision. For example, with a critical dimension simulation variability of 5% ( $1\sigma$ ), the best average matching and extra rates are 73.6% and 26.4% respectively.<sup>36</sup> More stringent accuracy specifications than such theoretical bounds are unrealistic.

#### 3.3 Electrical DFM

From a full-chip image lithography contours can be derived. By employing a suitable wire delay or transistor model such as BSIM,<sup>37</sup> electrical performance can be calculated and fed back for OPC or layout enhancement. Such electrical DFM approach was shown to be viable from the computational standpoint.<sup>38</sup> Specifications for these applications, however, must consider all factors that significantly affect electrical behavior, an example being the possible interaction between corner-rounding effects and oxidation-induced stress effects. Should stress effects be found to be of higher relative importance, contour-to-electrical DFM may not make full engineering sense.

### 4 Remarks

If we consider a plane with the  $x$ -axis denoting the degree of engineering sensible-ness and the  $y$ -axis representing performance requirement (defined by some combination of turn-around, accuracy, and precision

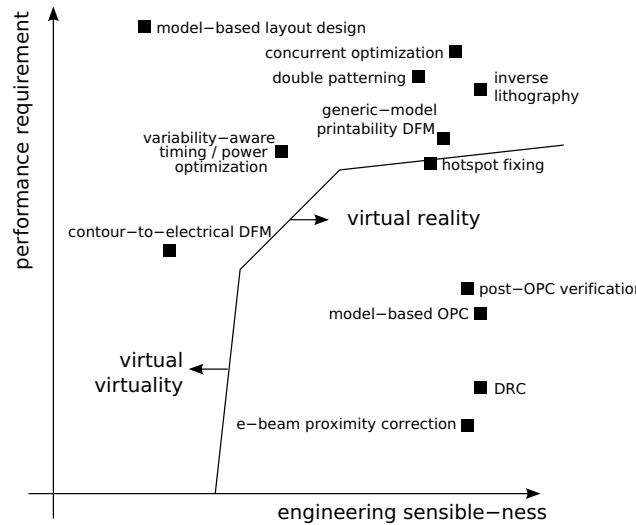


Figure 2: The reality-virtuality space of computation lithography (not to scale).

metrics), we can demarcate the plane into two areas. The one to the lower-right of the dividing line is the realm of virtual reality, while the region to the upper-left is the region of virtual virtuality. Applications can be placed onto this plane according to their degrees of reality, as illustrated in Fig. 2.

With algorithmic innovation and increased parallelization, the boundary between reality and virtuality will evolve. Today's virtuality can become tomorrow's reality. Simultaneously, with enhancements in our understanding and as requirements scale with technology, the markers also travel on their own trajectories. For example, lithography model accuracy needs to improve with decreasing critical dimension, pushing the "model-based OPC" marker upwards in the graph. Today's reality may become tomorrow's virtuality.

For computation lithographers, the goals are to enlarge the virtual reality region and to push the markers towards the lower-right. In this regard, applications on the right side of Fig. 2 around the reality envelope deserve special attention.

## References

- [1] F. H. Dill, W. Hornberger, P. Hauge, and J. Shaw, "Characterization of positive photoresists," *IEEE Transactions on Electron Devices*, vol. ED-22, pp. 445–452, July 1975.
- [2] K. L. Konnerth and F. H. Dill, "In-situ measurement of dielectric thickness during etching or developing process," *IEEE Transactions on Electron Devices*, vol. ED-22, pp. 452–456, July 1975.
- [3] F. Dill, "The basis for lithographic modeling," in *Proc. SPIE* (B. W. Smith, ed.), vol. 5754, pp. 377–382, 2005.
- [4] C. A. Mack, "Thirty years of lithography simulation," in *Proc. SPIE* (B. W. Smith, ed.), vol. 5754, pp. 1–12, 2005.
- [5] A. Neureuther, "If it moves, simulate it!," in *Proc. SPIE* (H. J. Levinson and M. V. Dusa, eds.), vol. 6924, p. 692402, 2008.
- [6] M. Yeung, "Modeling aerial images in two and three dimensions," in *Proc. Kodak Microelectronics*, pp. 115–126, 1985.
- [7] D. Nyssonen and C. P. Kirk, "Optical microscope imaging of lines patterned in thick layers with variable edge geometry: theory," *J. Opt. Soc. Am. A*, vol. 5, pp. 1270–1280, Aug. 1988.
- [8] K. Lucas, C.-M. Yuan, and A. Strojwas, "A rigorous and practical vector model for phase shifting masks in optical lithography," in *Proc. SPIE* (J. D. Cuthbert, ed.), vol. 1674, pp. 252–263, 1992.
- [9] T. Matsuzawa, A. Moniwa, N. Hasegawa, and H. Sunami, "Two-dimensional simulation of photolithography on reflective stepped substrate," *IEEE Transactions on Computer-aided Design of Integrated Circuits and Systems*, vol. 6, pp. 446–451, May 1987.
- [10] H. P. Urbach and D. A. Bernard, "Modeling latent image formation in photolithography using the Helmholtz equation," in *Proc. SPIE* (V. Pol, ed.), vol. 1264, pp. 278–293, 1990.
- [11] K. S. Yee, "Numerical solution of initial boundary value problems involving Maxwell's equations in isotropic media," *IEEE Transactions on Antennas Propagation*, vol. 14, pp. 302–307, May 1966.
- [12] R. Guerrieri, K. H. Tadros, J. Gamelin, and A. Neureuther, "Massively parallel algorithms for scattering in optical lithography," *IEEE Transactions on Computer-aided Design of Integrated Circuits and Systems*, vol. 10, pp. 1091–1100, Sept. 1991.

- [13] J. A. Sethian, "Fast marching level set methods for three-dimensional photolithography development," in *Proc. SPIE* (G. Fuller, ed.), vol. 2726, pp. 262–272, 1996.
- [14] S. Osher and J. A. Sethian, "Fronts propagating with curvature-dependent speed: Algorithms based on Hamilton-Jacobi formulations," *Journal of Computational Physics*, vol. 79, pp. 12–49, 1988.
- [15] J. F. Chen, T. Laidig, K. Wampler, and R. Caldwell, "Optical proximity correction for intermediate-pitch features using sub-resolution scattering bars," *J. Vac. Sci. Technol. B*, vol. 15, pp. 2426–2433, Nov. 1997.
- [16] O. Otto and R. Henderson, "Advances in process matching for rules-based optical proximity correction," in *Proc. SPIE*, vol. 2884, pp. 425–434, 1996.
- [17] N. Cobb and A. Zakhor, "Experimental results on optical proximity correction with variable threshold resist model," in *Proc. SPIE* (G. Fuller, ed.), vol. 3051, pp. 458–468, 1997.
- [18] M. Rieger and J. Stirniman, "Mask fabrication rules for proximity corrected patterns," in *Proc. SPIE*, vol. 2884, pp. 323–332, 1996.
- [19] T. Waas, H. Eisenmann, and H. Hartmann, "Proximity correction for high CD-accuracy and process tolerance," in *Proc. Symposium on Nanocircuit Engineering*, 1994.
- [20] H.-Y. Liu, L. Karklin, Y.-T. Wang, and Y. C. Pati, "Application of alternating phase-shifting masks to 140 nm gate patterning II: Mask design and manufacturing tolerances," in *Proc. SPIE*, vol. 3334, pp. 2–14, 1998.
- [21] H. Gamo, "Matrix treatment of partial coherence," in *Progress in Optics* (E. Wolf, ed.), vol. 3, pp. 187–332, North-Holland, 1964.
- [22] Y. C. Pati, A. A. Ghazanfarian, and R. F. Pease, "Exploiting structure in fast aerial image computation for integrated circuit patterns," *IEEE Transactions on Semiconductor Manufacturing*, vol. 10, pp. 62–74, Feb. 1997.
- [23] A. E. Rosenbluth, G. Gallatin, R. Gordon, W. Hinsberg, J. Hoffnagle, F. Houle, K. Lai, A. Lvov, M. Sanchez, and N. Seong, "Fast calculation of images for high numerical aperture lithography," in *Proc. SPIE* (B. Smith, ed.), vol. 5377, pp. 615–628, 2004.
- [24] M. Born and E. Wolf, *Principles of Optics*, pp. 491–555. Pergamon Press, sixth ed., 1980.
- [25] J. W. Goodman, *Introduction to Fourier Optics*. Roberts and Company, third ed., 2004.
- [26] A. K. Wong, *Resolution Enhancement Techniques in Optical Lithography*. SPIE Press, 2001.
- [27] A. K. Wong, *Optical Imaging in Projection Microlithography*. SPIE Press, 2005.
- [28] J. Kim and M. Fan, "Hotspot detection on post-OPC layout using full-chip simulation-based verification tool: a case study with aerial image simulation," in *Proc. SPIE* (K. R. Kimmel and W. Staud, eds.), vol. 5256, pp. 919–925, Dec. 2003.
- [29] S. D. Shang, Y. Granik, N. B. Cobb, W. Maurer, Y. Cui, L. W. Liebmann, J. M. Oberschmidt, R. N. Singh, and B. R. Vampatella, "Failure prediction across process window for robust OPC," in *Proc. SPIE* (A. Yen, ed.), vol. 5040, pp. 431–440, June 2003.
- [30] L. Pang, Y. Liu, and D. Abrams, "Inverse lithography technology (ILT): What is the impact to the photomask industry?," in *Proc. SPIE* (M. Hoga, ed.), vol. 6283, p. 62830X, Apr. 2006.
- [31] S. H. Chan, A. K. Wong, and E. Y. Lam, "Initialization for robust inverse synthesis of phase-shifting masks in optical projection lithography," *Optical Express*, vol. 16, pp. 14746–14760, Sept. 2008.
- [32] A. Poonawala and P. Milanfar, "Mask design for optical microlithography—an inverse imaging problem," *IEEE Transactions on Image Processing*, vol. 16, pp. 774–788, Mar. 2007.
- [33] B. Yenikaya and A. Sezginer, "A rigorous method to determine printability of a target layout," in *Proc. SPIE* (A. K. K. Wong and V. K. Singh, eds.), vol. 6521, p. 652112, Mar. 2007.
- [34] A. E. Rosenbluth, S. Bukofsky, C. Fonseca, M. Hibbs, K. Lai, A. F. Molless, R. N. Singh, and A. K. K. Wong, "Optimum mask and source patterns to print a given shape," *Journal of Microlithography, Microfabrication, and Microsystems*, vol. 1, pp. 13–30, Apr. 2002.
- [35] H. Mashita, T. Kotani, F. Nakajima, H. Mukai, K. Sato, S. Tanaka, K. Hashimoto, and S. Inoue, "Tool-induced hotspot fixing flow for high volume products," in *Proc. SPIE*, vol. 7028, p. 70283I, 2008.
- [36] A. K. K. Wong and E. Y. Lam, "The nebulous hotspot," in *Proc. SPIE*, vol. 7275, 2009.
- [37] J. H. Huang, Z. H. Lui, M. C. Jeng, P. K. Ko, and C. Hu, "A robust physical and predictive model for deep-submicrometer MOS circuit simulation," Master's thesis, University of California, Berkeley, May 1993. Memorandum No. UCB/ERL M93/57.
- [38] S. Banerjee, P. Elakkumanan, L. W. Liebmann, J. A. Culp, and M. Orshansky, "Electrically driven optical proximity correction," in *Proc. SPIE* (V. K. Singh and M. L. Rieger, eds.), vol. 6925, p. 69251W, 2008.